Optical Fibre Fabry-Perot Interferometers for Calorimetric Heat Transfer Gauges

S.R. Kidd, J.S. Barton, J.D.C. Jones
Heriot-Watt University, Edinburgh, UK

K.S. Chana, I.W. Matthews
DRA Farnborough, UK

1. Abstract

A heat flux measurement system comprising a laser diode, a single mode optical fibre interferometer and passive optical fibre components has been constructed. The system has been designed for use in transient flow wind tunnels and has a resolution of 1 kW m^{-2} , a dynamic range of 20 MW m^{-2} and bandwidth > 100 kHz. Heat flux measurements have been made with the system on the endwall of a cascade of stator blades.

2. Introduction

In this paper we describe a laser based fibre interferometer system for measuring heat transfer rates. The technique is intended for application in making heat flux measurements via transient methods such as in short duration (~20 ms) blowdown wind tunnels and longer duration (≤ 1s) pulsed wind tunnels.

Current techniques for heat transfer measurement include liquid crystals (Ireland & Jones 1986), mass transfer analogues (Heikal et al. 1991) and swollen polymers (Roberts et al. 1991). In addition, platinum thin film resistance gauges (Schultz and Jones 1973) continue to play an important role in heat transfer measurements.

The potential advantages of a fibre optic sensor for heat transfer measurement are (i) high spatial resolution (~20μm^2), (ii) high temperature resolution (sub mK), (iii) intrinsic calibration, (iv) high measurement bandwidth (>100 kHz), (v) multiplexed arrays possible, and (vi) immunity to electro-magnetic interference.

The basic optical sensor design is that of a fibre Fabry-Perot (FFP) interferometer. In the sensor, a

short length of fibre (~2mm) with a low reflectivity coating at each end forms an interferometer.

In the following sections of this paper we shall describe the design, theory of operation, construction, operation and wind tunnel evaluation of FFP's as high bandwidth high resolution heat transfer gauges.

3. Sensor Operating Pinciples

3.1 The Fibre Fabry-Perot Interferometer

A fibre Fabry-Perot (FFP) interferometer can be formed inside a length of single mode optical fibre simply by cleaving the ends of the fibre normal to the propagation axis. Each cleaved end provides a Fresnel reflection of ~ 4 %. The single mode propagation property of the fibre provides only one optical path between the fibre ends and thus results in the possibility of a resonant cavity for optical radiation (at one appropriate wavelength and given suitable temporal coherence properties of the radiation).

If a second length of single mode fibre is placed so that it butt joins the FFP, as shown in figure 1, then the FFP can be efficiently illuminated. This second fibre (termed the addressing fibre) can also return the light reflected from the FFP to a suitable detection system.

Vaughan (1989) gives full details of the Fabry-Perot resonator : only the briefest outline is given here. The intensity of the returned light is dependent on the optical phase ϕ associated with one round trip of the FFP, such that

$$\phi = \frac{4\pi n l}{\lambda} \tag{1}$$

where n is the effective refractive index of the fibre core, l is the length of the FFP and λ is the wavelength of the illuminating light. The phase is thus directly proportional to the optical length of the interferometer. As ϕ changes, the reflected and transmitted FFP intensity changes, giving rise to a series of interference fringes. For the case of low reflectivity at each end of the FFP, only the lowest order reflections need be considered, and the return intensity I is then given by

$$I = I_M(1 + V\cos\phi) \tag{2}$$

where I_M is the mean return intensity (averaged over one period of cos ϕ) and V is the visibility of the fringe pattern, where

$$V = \frac{I_{MAX} - I_{MIN}}{I_{MAX} + I_{MIN}} \tag{3}$$

and where I_{MAX} and I_{MIN} are the fringe intensity maxima and minima.

3.2. The FFP as a sensor

The basis of the FFP as a sensor is that the single mode fibre from which it is constructed has an intrinsic phase sensitivity to temperature, pressure and strain -

$$\frac{\Delta\phi}{\phi} = \frac{1}{\phi}\frac{\partial\phi}{\partial T}\Delta T + \frac{1}{\phi}\frac{\partial\phi}{\partial P}\Delta P + \frac{1}{\phi}\frac{\partial\phi}{\partial\varepsilon}\Delta\varepsilon \tag{4}$$

where T, P and ε represent temperature, pressure and strain respectively. For the fused silica core fibre used in our experiments in wind tunnels, it has been shown (Hocker 1979) that the thermal phase sensitivity of the fibre dominates over the pressure and strain sensitivities in many practical situations. From equation (1), we see that the thermal sensitivity of a short length of fibre in thermal equilibrium is given by

$$\frac{\partial\phi}{\partial T} = \frac{4\pi}{\lambda}\left(n\frac{\partial l}{\partial T} + l\frac{\partial n}{\partial T}\right) \qquad (5)$$

or

$$\frac{1}{l}\frac{\partial\phi}{\partial T} = \frac{4\pi}{\lambda}(n\alpha+\beta) \qquad (6)$$

where α is the thermal expansivity of the fibre, and β = dn/dT is the thermo-optic coefficient. For the fused silica fibre used in our experiments, the term in β dominates.

With appropriate signal processing (Culshaw & Dakin 1989), it is possible to convert from changes of FFP reflected intensity to changes of phase using equation (2). Then, using the first term of equation (4), the temperature change can be determined.

3.3. The FFP as a calorimeter

The FFP can be used as a calorimeter in transient wind tunnel experiments by embedding it in a substrate (e.g. a model turbine blade under test) such that its length l is perpendicular to the substrate surface, as shown in figure 2 with its distal (outer) face flush with the surface. Fused silica, from which the optical fibres were fabricated, has thermal properties very similar to those of machinable ceramics (e.g. Macor), from which model test components designed for use with platinum thin film gauges are most commonly made. Hence, a one dimensional heat transfer model is sufficient to describe heat flow in the substrate and FFP. An advantage of the optical gauge is that it is all-dielectric, and may hence be used with electrically conducting (e.g. metal) test components. In this case, a two dimensional heat transfer analysis is required, but the mode of operation is similar.

The timescale over which the FFP can operate as a calorimeter is set by its length. The length l must be long compared to the depth of penetration of a heat pulse incident as a plane wave parallel to the substrate surface and FFP distal face. This depth can be taken as the thermal diffusion depth D_t for an incident heat pulse of duration t.

$$D_t = 4\sqrt{\gamma t} \qquad (7)$$

where γ is the thermal diffusivity of the fused silica of the FFP. For $l \geq D_t$ a negligible proportion of the thermal wave of the incident heat pulse propagates as far as the proximal (inner) face of the FFP. An FFP 3mm long constructed from fused silica with $\gamma = 8.4 \times 10^{-7}$ m^2s^{-1} is suitable for calorimetric operation in wind tunnels with a pulse duration of up to 0.5 s.

The phase change $\Delta\phi$ of the FFP associated with a temperature change ΔT relative to uniform ambient temperature of T_o is

$$\Delta\phi = \phi(T_o + \Delta T) - \phi(T_o) \qquad (8)$$

For the case in which the temperature change is a function of distance along the fibre core, equation (8) becomes

$$\Delta\phi = \frac{4\pi(n\alpha+\beta)}{\lambda}\int_0^l \Delta T(x)\, dx \qquad (9)$$

where $\Delta T(x)$ is the temperature change of an elemental length dx of the FFP. If $\overline{\Delta T}$ is defined as the mean temperature rise integrated over the length of the FFP, then equation (9) becomes

$$\Delta\phi = \frac{4\pi(n\alpha+\beta)l\overline{\Delta T}}{\lambda} \qquad (10)$$

The calorimeter equation in terms of $\overline{\Delta T}$ applied to the FFP is

$$q = \rho C l \overline{\Delta T} \qquad (11)$$

where ρ and C are the mass density per unit length and specific heat capacity of fused silica respectively and q is the heat energy gained by the calorimeter per unit cross-sectional area. Taking the time derivative of equation (11) and substituting using equation (10) yields the surface heat transfer rate in terms of the phase change of the FFP

$$\dot{q} = \frac{\rho C \lambda}{4\pi(n\alpha+\beta)} \frac{d\phi}{dt} \qquad (12)$$

It can be seen from this equation that the calibration of the FFP to measure heat flux in Wm^{-2} is intrinsic, dependent only on the properties of fused silica and the wavelength of light used to illuminate the FFP, and is independent of the length of the sensor.

4. The Measurement System

Figure 3 is a schematic representation of the complete measurement system that we have constructed. Light from a laser diode (Sharp LTO24) operating with a mean optical power of 20 mW at a wavelength of 780 nm is coupled into arm 1 of a single mode fibre directional coupler (DC). This light is split in a 50/50 power ratio between the two output arms 2 and 4. Arm 2 is spliced to the addressing fibre, which can be of arbitrary length (up to 100m in our experiments). The FFP reflection returns to the directional coupler where it is split between arms 1 and 3. A photo-diode at the end of arm 3 is used to monitor the return intensity. In principle arm 4 of the DC is not needed, but we have used the signal in this arm as an intensity reference to allow compensation for laser intensity noise and variations in the laser-to-fibre launch efficiency. The output from the photo-detectors is captured with a transient recorder.

For heat transfer experiments where only a small optical phase change (<< π rads) is induced in the FFP, signal processing is straightforward. In this regime, the FFP reflected intensity is linearly related to FFP phase, provided the initial phase of the FFP is not close to a turning point of equation (2). This initial phase setting can be achieved by control of the laser diode wavelength via its injection current (Dandridge & Goldberg 1982).

For cases where the FFP phase varies over a significant fraction of 2π rads, an alternative technique is required to avoid signal fading. We have chosen a technique based on quadrature switching the laser diode wavelength, again by controlling its injection current. This effectively generates two wavelengths (λ_1 and λ_2) of illumination of the FFP, each wavelength being used alternately. The wavelength difference λ_1-λ_2 is chosen so that the FFP phase (given by equation (1)) shifts by π/2 as a result of the change in wavelength. The reflected signals from the FFP can then be described as

$$I_1 = I_{M1}(1 + V \sin\phi) \qquad (13)$$

$$I_2 = I_{M2}(1 + V \cos\phi) \qquad (14)$$

From equations (13) and (14) it possible to obtain a unique value of φ that does not suffer from signal fading. Using this technique we have quadrature switched the laser diode source at rates of up to 10 kHz (Anderson et al. 1991), though the potential for higher switching rates of up to at least 90 kHz exists.

A multiplexed sensor system of up to 4 sensors has been constructed and operated by us. The basic single channel system of figure 3 has been incorporated into a network of 7 fibre directional couplers as shown in figure 4. In this system, four sensors are illuminated from a single laser diode source and the reflected signal from each FFP is taken to a separate photo-detector.

5. Evaluation Experiments

Initial laboratory evaluation of the FFP sensors was carried out with pulsed heating experiments using a pulsed Nd:YAG laser (Kidd et al. 1990). From these experiments, a response time of the sensing system was established as < 8 μs. The FFP sensor was capable of measuring heat fluxes in the range 1 kWm^{-2} to 20 MWm^{-2} .

Pulsed wind tunnel sensor evaluation took place in a short duration shock tube, run in the Ludwieg configuration (Ludwieg 1957). A schematic of this tunnel is given in figure 5. Before each run, the main tube was pressurized to 8 Bar with argon and the dump tank evacuated to a rough vacuum. When the double diaphragms were burst by venting the intermediate volume to the atmosphere, an expansion wave propagated the length of the main tube. Behind this wave, the gas expanded, cooled and flowed through the working section to the dump tank, attaining a velocity of Mach 0.7 and a temperature of ~ 50 K below ambient. The run time of the tube was 20 ms.

A flat plate constructed of Macor with an elliptical leading edge was used as a simple test model and placed in the working section of the tube. It was instrumented with 4 FFP gauges embedded and cemented at different distances from the leading edge. There were also 6 platinum thin film gauges, 4 of which were located at distances from the leading edge corresponding to the FFP gauges. The thin film gauges provided comparison data for the heat transfer values obtained from the FFP gauges.

Given the thermal properties of Macor and the run conditions of the Ludwieg tube, heat flux from the plate to the cooler gas was anticipated to be between 40 kWm^{-2} and 100 Wm^{-2}, depending on the degree of turbulent flow over the plate. The anticipated change in the FFP calorimeter temperature was ~ 300 mK.

The Ludwieg tube was chosen as a particularly stringent test of the Fabry-Perot sensors, given that the duration of the heat pulse was short, leading to a small temperature signal, and the magnitude of the pressure change was large. Following these successful evaluations, further experiments were conducted in a more realistic practical situation using a transient flow wind tunnel of run duration 520 ms, with a mean fluid-to-blade temperature difference of 160 K, and a pressure change of 1.5 bar. Experiments were again conducted using a Macor blade instrumented with Fabry-Perot sensors.

For these experiments, the FFP mounting arrangements were modified such that the sensors were an accurate sliding fit within the substrate, rather than being cemented into place. It was believed that such an arrangement would prevent the communication of strain from the substrate to the sensor, thus reducing the apparent pressure cross-sensitivity. In the experiments, the optical arrangement for interrogating the sensor was situated at a distance of 10m from the tunnel, communicating via an optical fibre cable.

6. Evaluation Results

Figure 6 shows a typical result of a Ludwieg tube run. The run time of the tube is indicated by the region of the pressure trace that is constant. The mean heat transfer rate determined using the FFP gauge was 53 ± 6 kWm^{-2} and that of the corresponding thin film gauge was 52 ± 1 kWm^{-2}. A summary of further runs is given in the following table. Sensor number in the table relates to the distance from the leading edge of the plate. Confidence limits for the thin film gauges are ± 5%.

Run	FFP No.	$\dot{q}$ (kWm^{-2})	Pt. No.	$\dot{q}$ (kWm^{-2})
1	5	39.2 ± 5.5	4	50
2	5	44.8 ± 6.3	4	50
3	5	34.2 ± 4.8	4	46
4	3	32.9 ± 4.6	4	52
	5	39.4 ± 5.5	6	44.5
5	1	31.7 ± 4.4	3	45.5
	3	13.9 ± 1.9	4	46.5
	5	19.8 ± 2.8		
6	1	21.4 ± 3.0	3	47
	3	28.4 ± 4.0		

After run 5, the Macor plate was found to have fractured and was no longer lying with the plane of the plate parallel to the gas flow. This meant that there was not a uniform distribution of heat transfer over the area of the plate. We believe that the FFP heat transfer rates for runs 5 and 6 therefore should not necessarily correspond to thin film heat transfer rates.

Typical results from an experiment using the longer duration wind tunnel are shown in figure 7, plotted as mean temperature change against time. The flow conditions were adjusted to produce an approximately constant heat flux. The mean heat flux obtained with the FFP sensors was 137 ± 7 kWm^{-2} , compared with 148 ± 4 kWm^{-2} from thin film gauges, thus showing good agreement within experimental error. The results show that the FFP sensors had insignificant pressure cross-sensitivity.

7. Discussion

A comparison between the heat transfer rates obtained from the FFP gauges and the thin film gauges given in the table shows that there was reasonable agreement between the two in the first 3 runs. In the later runs it is evident that there are significant differences in the heat transfer rate obtained from the different sensor types. As mentioned above, this is thought to be due to the damaged plate. This damage took the form of several large and deep cracks across the plate surface. The accidental damage to the plate tested the robustness of the FFP sensors, which continued to operate satisfactorily, whilst a number of platinum thin film gauges failed.

Several aspects of figure 6 are worth commenting on. It should be noted that the total temperature change of the FFP during the entire Ludwieg tube run was only 300 mK. The pressure sensitivity of the FFP sensor was much higher than first

expected, based on estimates of the pressure sensitivity of fused silica fibre. However, the mounting arrangement of the sensor could significantly increase its sensitivity to pressure (Bucaro 1987).

The large periodic oscillations in the data from the FFP are attributed to oscillations of mechanical components used to enable the coupling of light from the laser diode source to the fibre. The intensity referencing scheme outlined above was unable to completely correct for these variations.

In the experiments carried out using the longer duration pulsed wind tunnel the combination of a higher thermal signal and improved sensor mounting and intensity referencing yielded data showing negligible pressure cross-sensitivity or intensity noise. The results obtained showed excellent agreement with the platinum thin film gauges.

The noise limit for the FFP heat transfer measurements is determined by the contribution to the detected signal from parasitic optical reflections and parasitic optical cavities within the fibre optic network. Such reflections were reduced by design features such as careful matching of the refractive indices of components, but there is a fundamental backscattered signal arising from light that has been coherently Rayleigh scattered in the addressing fibre. We have devised a technique based on high frequency modulation of the wavelength of the laser diode, which significantly reduces this effect, so that the entire system noise floor is below 30 mK in a 100 kHz bandwidth.

Further development of the FFP sensor as a heat transfer gauge and a thermal sensor will continue, with development of alternative multiplexing and signal processing schemes, as well as improvements in the construction of the FFP. By further reducing the noise floor of the system towards its fundamental limit and by limiting the measurement bandwidth, thermal measurements with μK resolution are possible.

8. Conclusions

Measurements of heat flux using a fibre optic interferometric sensor have been successfully carried out in a short duration wind tunnel facility. The sensor has a resolution of 1 kWm^{-2} and a dynamic range of > 20 MWm^{-2}, with a measurement bandwidth of 100 kHz.

9. Acknowledgements

This work has been partially supported by the Procurement Executive, Ministry of Defence, DRA Aerospace, Pyestock, Farnborough. The authors wish to thank Dr. S. P. Harasgama of ABB Power Generation, formerly of DRA Aerospace, for many useful discussions and Prof. T. V. Jones of Oxford University for providing the Macor plate and platinum thin film resisitance gauges.

10. References

Anderson, D.J., Jones, J.D.C., Sinha, P.G., Kidd, S.R.& Barton, J.S. 1991 Scheme for Extending the Bandwidth of Injection Current Induced Laser

Diode Optical Frequency Modulation J.Mod. Opt. vol 38, pp 2459-2465

Bucaro J.A., 1987 Optical Fiber Sensor Coatings. Optical Fibre Sensors, NATO ASI Series E, no 132, pp321-338, Martinus Nijhoff, Dordrecht

Culshaw, B. & Dakin, J. 1989 Optical Fiber Sensors. ch 14, Artech House, Norwood, USA

Dandridge, A. & Goldberg L. 1982 Current Induced Frequency Modulation in Diode Lasers. Electron. Lett. vol 18 pp 302

Heikal, M.R., Cowell, T.A. & Ewles, J.D. 1991 Measurement of local and Average Heat Transfer Coefficients Using the Thin Film Mass Transfer Analogue and Video Image Processing Techniques. Proc. Eurotherm Seminar No. 25, Pau, France, pp 20-25

Hocker, G.B. 1979 Fiber-Optic sensing of pressure and temperature. App. Optics, vol 18, no 9, pp 1445-1448

Ireland, P.T. & Jones, T.V. 1986 Detailed Measurements of Heat Transfer on and Around a Pedestal in a Fully Developed Channel Flow. Proc. 8th Int. Heat Transfer Conf., San Fransisco, vol 3. pp 975-980

Kidd, S.R., Sinha, P.G., Barton, J.S. & Jones, J.D.C. 1990 Miniature Fast Response Temperature Sensors. Applied Optics Digest, Proc. Applied Optics and Opto-Electronics, IOP, Nottingham UK, pp 41-42

Ludwieg H, 1957 Tube Wind Tunnel, a Special Type of Blowdown Tunnel, NATO AGARD Report 143

Roberts, C.A., Grigris, N.S., Leech, J.R. & Viney I.V.F. 1991 Heat Transfer at Complex Surfaces Using a Swollen Polymer and Projected Optical Fringes. Proc. Eurotherm Seminar No. 25, Pau, France, pp 14-19

Schultz, D.L. & Jones, T.V. 1973 Heat Transfer Measurements in Short Duration Hypersonic Facilities. AGARD Report No. AG165

Vaughan, J.M. 1989 "The Fabry-Perot Interferometer, History, Theory, Practice and Applications," Adam Hilger, IoP Publishing Ltd.

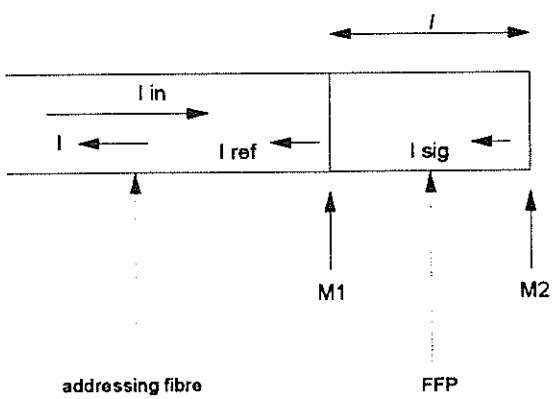

Figure 1

An optical Fibre Fabry-Perot (FFP) interferometer and addressing fibre

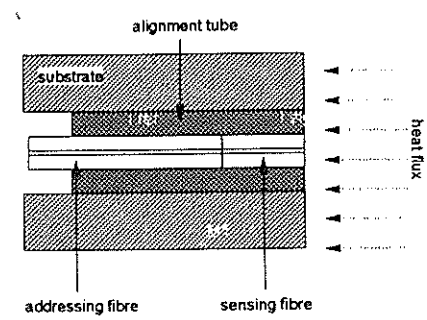

Figure 2

Cross section of optical fibre heat transfer sensor embedded within the test object substrate

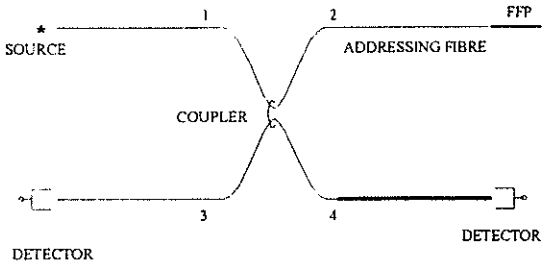

Figure 3

Optical system for a single heat transfer sensor

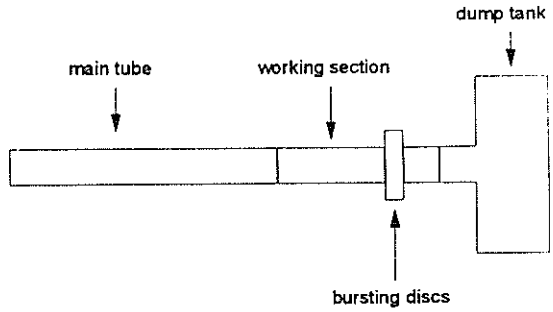

Figure 5

Schematic of the Ludwieg tube short duration wind tunnel

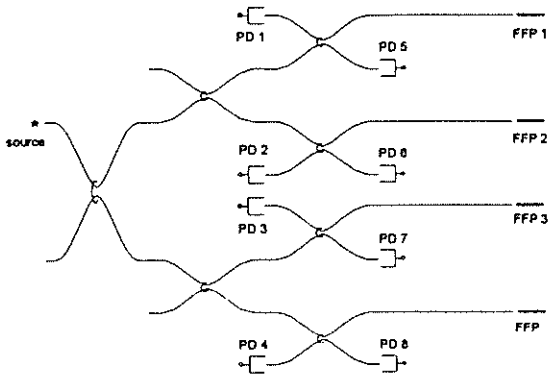

Figure 4

Fibre network for spatial multiplexing of four fibre Fabry-Perot heat transfer sensors FFP 1..4. PD 1..4 are the signal detectors, PD 5..8 are the corresponding reference detectors

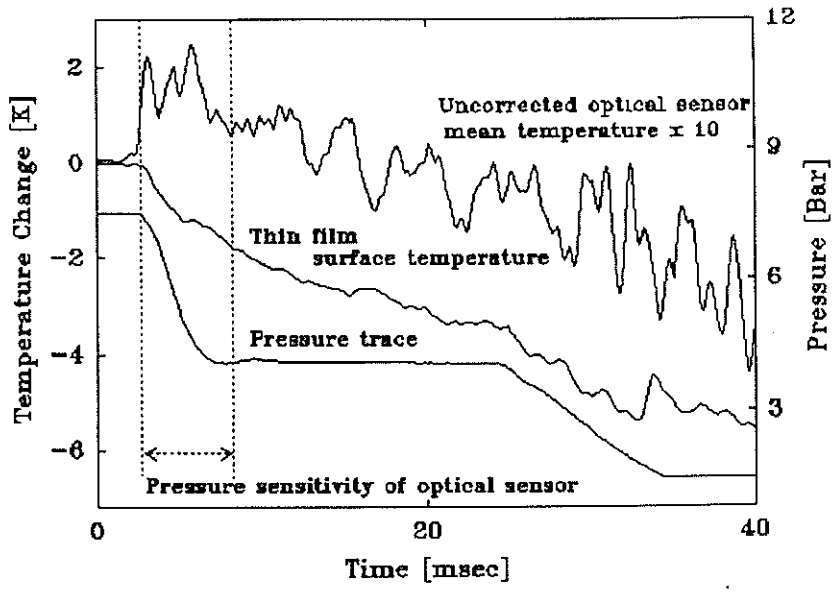

Figure 6

A typical result from a Ludwieg tube run, showing thin film gauge, pressure and FFP data

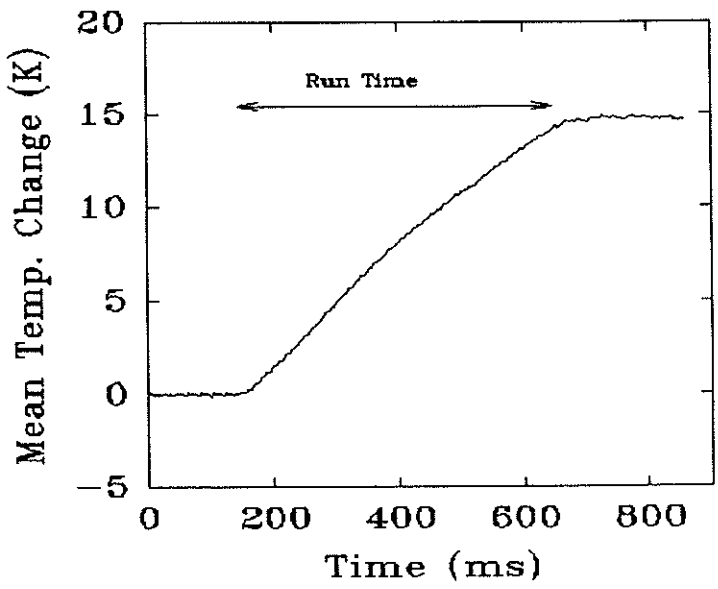

Figure 7

A result from a longer duration (~500ms) pulsed wind tunnel. The mean temperature change of the FFP calorimeter is plotted as a function of time